Supplementary Information

In-Situ Study of Molecular Structure of Water and Ice Entrapped in Graphene Nanovessels

Seyed Mohammadreza Ghodsi,[†] Sushant Anand,[‡] Reza Shahbazian-Yassar, [‡] Tolou Shokuhfar,[*,†] and Constantine M. Megaridis[*,‡]

[†] Department of Bioengineering, University of Illinois at Chicago, Chicago, IL 60607, United States

[‡] Department of Mechanical and Industrial Engineering, University of Illinois at Chicago, Chicago, IL 60607, United States

*tolou@uic.edu, cmm@uic.edu

GLC Fabrication

For proper GLC sealing, the layers of graphene should come in touch so that they tightly wrap around the sample.[1] Although this could be achieved using a single graphene sheet, we adopted the two-layer GLC fabrication technique to avoid further chemical functionalization of the graphene layers.[2,3] In this method, a 100µl droplet of DI water is squeezed between two sheets of graphene, as described below. The strong Van der Waals forces between the dry graphene layers, seal around the liquid sample to form nano- to micro-sized pockets of water on the TEM grid. Leaving the sample in vacuum overnight further assists to bring the two graphene sheets closer by purging the excess amount of water, thus resulting in more robust GLCs. Studies have shown that heating the sample to the melting point of the TEM grid (~1000°C) has the same effect.[4]

The steps for fabricating a typical GLC are as follows (Figure S1):

1. Cut graphene-suspending copper substrate to small pieces (~cm^2).
2. Float the graphene-contained copper substrate on the etchant solution ($(NH_4)_2S_2O_4$ or $FeCl_3$) for several hours.
3. Locate the free-standing graphene on the etchant solution.
4. Lift the graphene layer using a clean glass slide or an etchant-resistant loop.[5]
5. Transfer the graphene layer on DI water to remove etchant remnants from the surface of graphene.
6. Harvest free-standing graphene with TEM grid to form graphene-coated grids.
7. Load the hydrated specimen on the graphene side of a graphene-covered TEM grid.
8. Harvest second graphene layer with specimen-loaded TEM grid to entrap a thin film of liquid specimen between two graphene layers.
9. Leave the fabricated GLC in desiccator overnight to evaporate the excess amount of liquid.

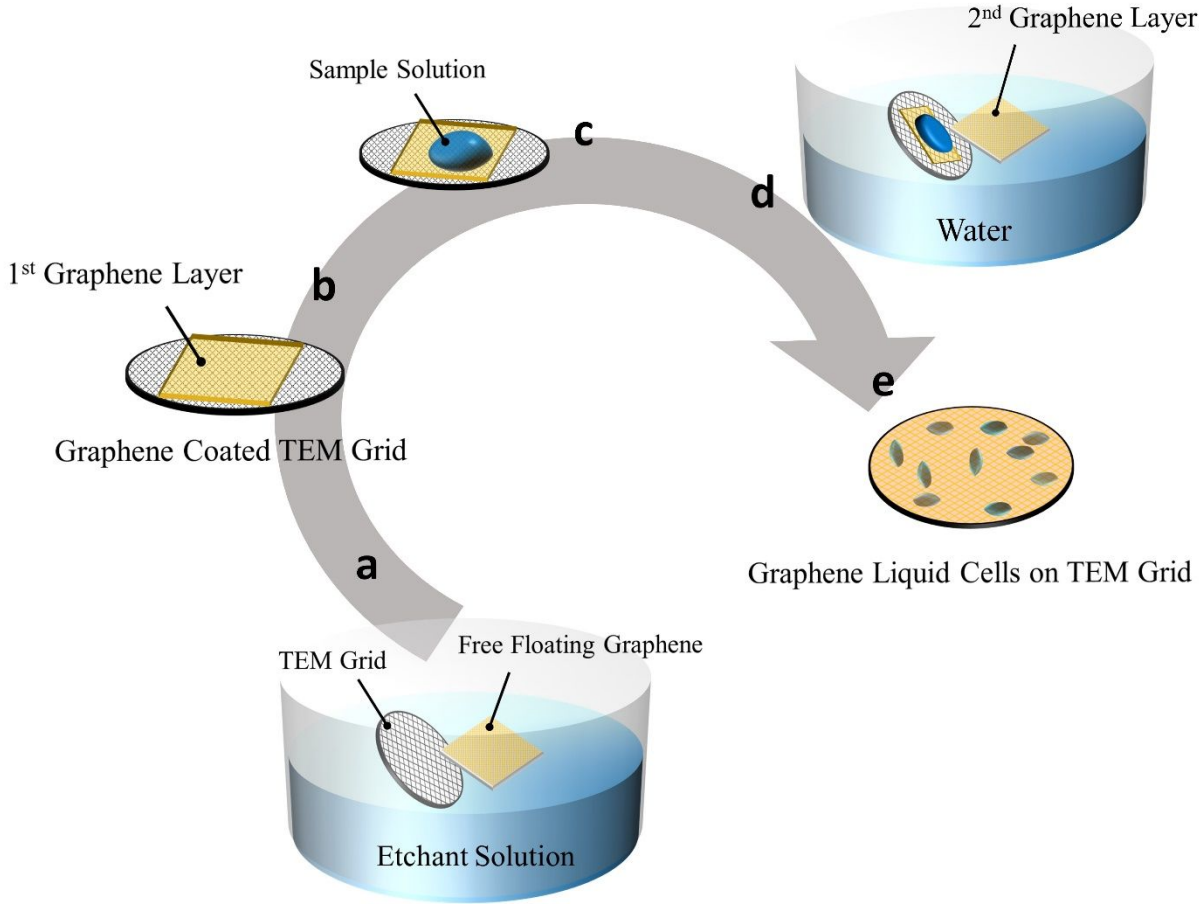

Figure S1. *Fabrication of GLC specimen:* Graphene/copper substrate stays afloat on the ammonium persulfate etchant solution to remove copper. Free-floating graphene is then washed with DI water (not shown) and transferred onto a TEM grid (b). After the deposition of the hydrated sample on the graphene-coated grid (c), a second graphene layered is deposited on the grid to form GLCs (d). A successful GLC fabrication results in numerous graphene-encased liquid pockets on the TEM grid with various sizes and thicknesses (e).

Beam Heating

The beam-induced temperature rise of the specimen is estimated by[6,7]

$$\Delta T = \frac{I_b \ \ dE}{2\pi\kappa e\, dx} \ln\left(\frac{\pi a}{2d}\right)$$

where I_b is the beam current (100pA), the rate of energy-loss per electron $\frac{dE}{dx}$ is around 0.04 $\frac{eV}{nm}$, κ is the thermal conductivity of water (0.5 $\frac{W}{mK}$) and a, d are field-of-view dimensions ($a \approx d$).[6] Thus, ΔT is estimated to be about 0.1K, which is negligible.

Mitigating Radiolysis Defect in GLC

While the content of the GLC is always susceptible to radiolysis, reducing the electron beam current mitigates the defects of dissolved electrons and radicals on the fluid specimen. Herein, after identifying the subject GLC in the Ronchigram mode, STEM mode was performed with 5µA beam-current and 40µm objective aperture, which reduced the current further down to 100pA.[8] The electron beam intensity was estimated to be around 0.3 $e\ \text{Å}^{-2}s^{-1}$ on the specimen, which is well below the critical intensity threshold.[9] Figure S2 depicts a specimen after three successive EELS spot measurements; the stability of the liquid-free portion (bubble) in the GLC confirms the resilience of the sample in the low-dose electron beam. The electron current density was kept the same on the specimen at cryogenic temperature to minimize the radiation damage.

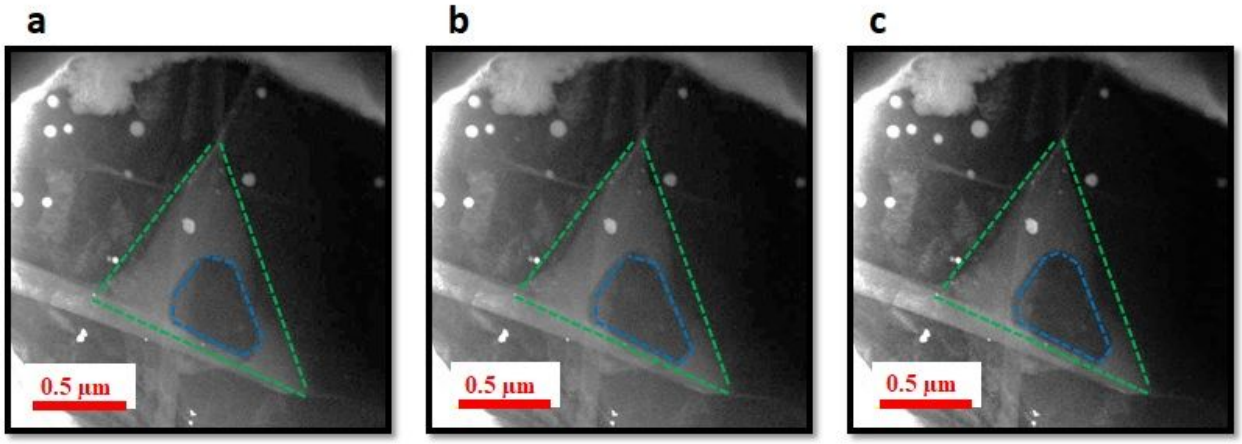

Figure S2. *Snapshots of a typical GLC (green-dashed boundary) during multi-spot EELS examination*. The stability of a bubble (blue-dashed boundary) inside the GLC shows that radiolysis had no detectable effect at the low-dose condition of this experiment. Scale bar denotes 500nm.

Oxygen Core-Loss Electron Energy-Loss Spectroscopy of Dry and Wet Graphene Cells

A comparison between the EELS data for dry and wet graphene cells indicates negligible contribution of graphene to the oxygen K-edge core-loss peak of GLC (Figure S3). While the pre- and post-edges of oxygen core-loss in water oscillates with GLC temperature and wall-spacing variation, the oxygen core-loss of graphene remains unchanged.

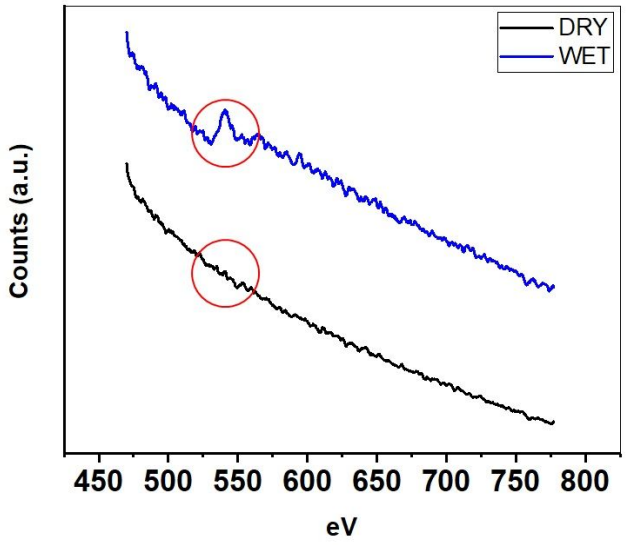

Figure S3. *The oxygen K-edge core-loss peak in wet and dry graphene enclosures before background subtraction*. While water makes a significant enhancement in the oxygen core-loss peak intensity of the GLC, graphene sheets make a negligible contribution.

Low-Loss EELS of Water GLC at -165°C

Confinement thickness of the designated spots in Fig. 1 were derived using low-loss spectra across GLC samples at room and cryogenic temperatures. While all the low-loss spectra of GLC at room temperature were shown in Fig. 1, the spectra for cryogenic temperature are shown in Fig. S4.

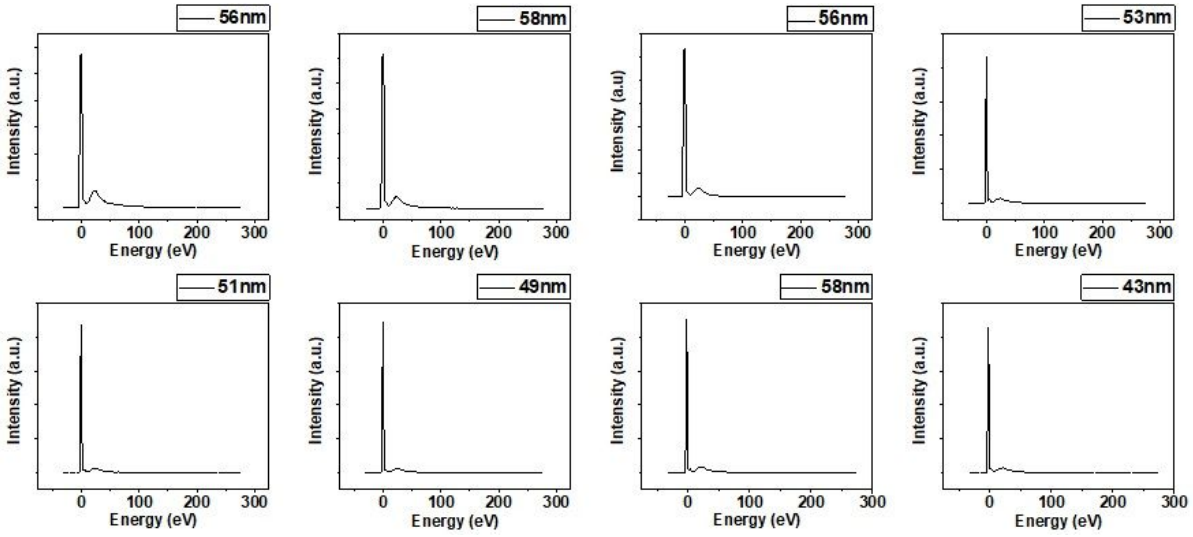

Figure S4. *Low-loss EELS spectra of water encased in GLC at - 165°C.* Low-loss EELS spectra were used to estimate the confinement thickness of the sample.

Core-Loss EELS of Water GLC at -165°C

The oxygen core-loss spectra of GLCs at room and cryogenic temperatures were used to derive the structural index of graphene-encapsulated water. While all the oxygen core-loss spectra of GLC at room temperature were shown in Fig. 3, the spectra at cryogenic temperature are shown in Fig. S5.

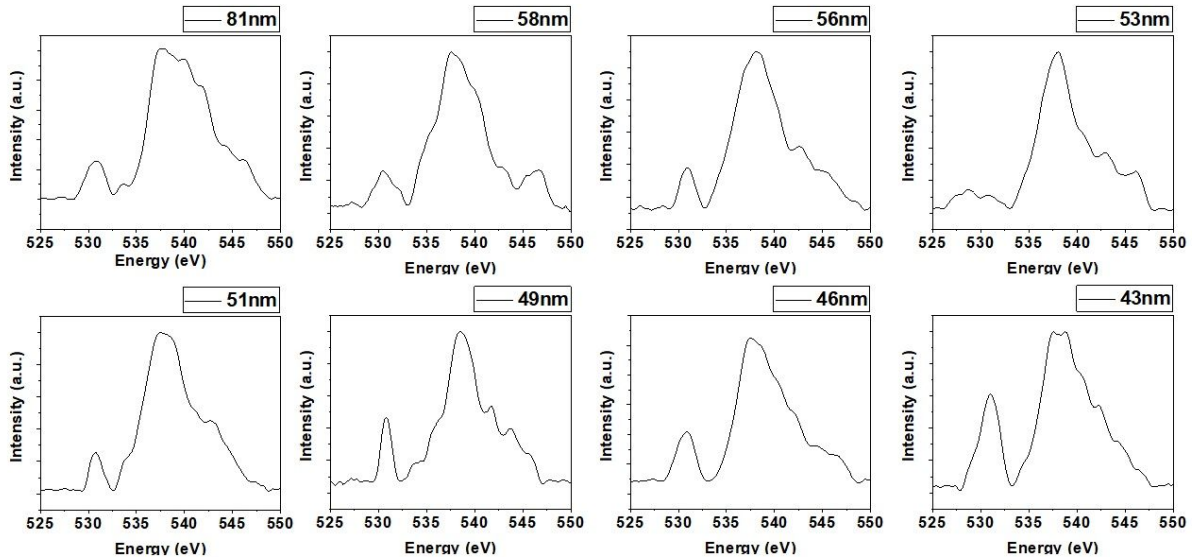

Figure S5. *Core-Loss EELS of water encased in GLC at -165°C.* Low-loss EELS spectra were used to estimate the structural index of tightly-encapsulated water.

Core-Loss EELS Curve Fitting

OriginPro™ data analysis and graphing software was used to fit the EELS curves in Fig. 3. The peak position, peak intensity and baseline positions were determined freely by the software without specification of any particular peaks. The total number of peaks in each curve was fixed at 4 in Fig. 3a and 5 in Fig 3b with the resulting R^2 above 0.99 in all cases. Gaussian curve fitting in Fig. 3 was used to attain the position of different peaks in the oxygen core-loss spectra. The positions of fitted peaks are in good agreement with previously-reported soft X-ray spectra of water molecules.[10] The changes in relative heights of the oxygen peaks reflect the population ratio of different hydrogen bonding structures in our EELS spectra.[11] In order to minimize the systematic error introduced by the EELS energy resolution (0.7 eV), the area under each peak ± 1 eV was used to calculate these ratios.

EELS Energy Resolution

The energy resolution of EELS measurements were derived based on Full Width at Half Maximum (FWHM) of the zero-loss peak in Digital Micrograph™ suit.[12] The energy resolution was estimated to be 0.7 eV.

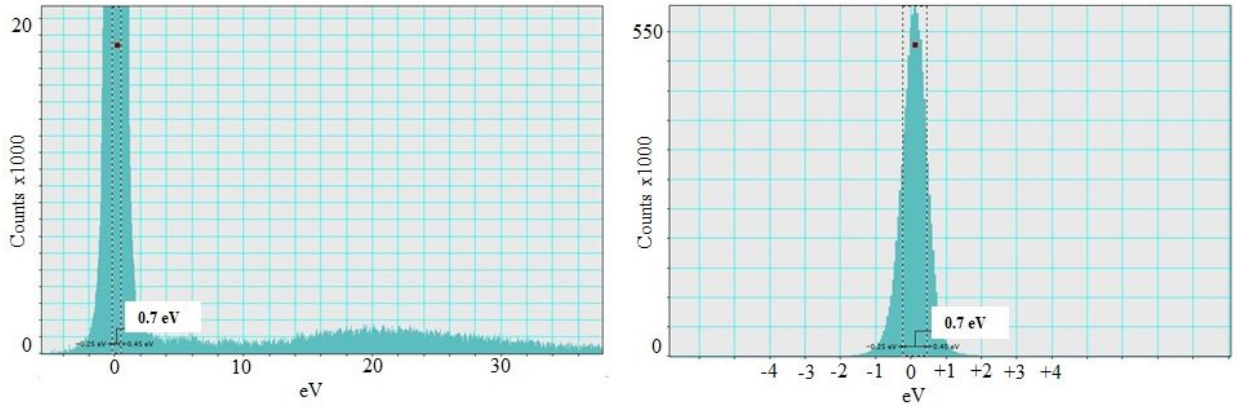

Figure S6. *Estimation of the EELS energy resolution using FWHM technique*. The sub-eV energy resolution of EELS makes *in-situ* study of encapsulated water in GLC pockets feasible.

Entropy of Q2D vs. 3D Regime

Studies have shown how reducing the wall spacing of entrapped water from 3D to Q2D, will replicate flat hexagonal bi-layers of water molecules (a.k.a Nebraska ice).[13] Figure S7 sketches the entropy of these two ice regimes (S) against the isotropic volume of the cell. The transition from 3D to Q2D takes place at V~0.08 nm^3 (t_z ~ 0.4 nm), which is comparable to 0.37 nm of ice bi-layer separation. Following the trend of changes in structural index attained by EELS shows that upon reducing the wall spacing below 1 nm, hydrogen bonding saturates. This finding is in good agreement with previously reported MD simulations, where it was shown that in the Q2D regime, ice bilayers form with saturated hydrogen bonding.[14]

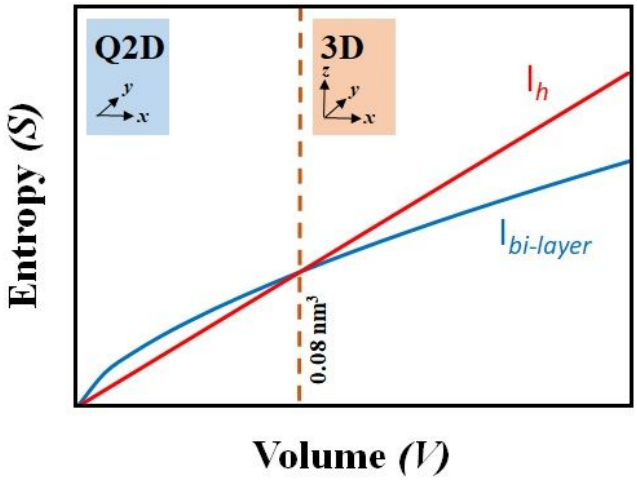

Figure S7. *Entropy of entrapped ice inside GLC nanovessels*. $S = k_B \ln \Omega$, where the partition function (Ω) is $2^{N/4}$ in Q2D amorphous ice and 1.5^N in hexagonal ice.[15–18] By moving from the Q2D area towards the center of the GLC nanovessel (3D), the hexagonal ice structure becomes more energetically favored (red) compared to flat hexagonal bi-layer ice (blue). The bi-layer ice forms instantaneously upon freezing,

while the hexagonal ice forms at the less-confined regions.

References

1. Ghodsi, S. M., Megaridis, C. M., Shahbazian-Yassar, R. and Shokuhfar, T. Advances in Graphene-Based Liquid Cell Electron Microscopy: Working Principles, Opportunities, and Challenges. *Small Methods*, **2019**, 1900026.
2. Mohanty, N. & Berry, V. Graphene-Based Single-Bacterium Resolution Biodevice and DNA Transistor: Interfacing Graphene Derivatives with Nanoscale and Microscale Biocomponents. *Nano Lett.* **2008**, 8, 4469–4476.
3. Textor, M. & De Jonge, N. Strategies for Preparing Graphene Liquid Cells for Transmission Electron Microscopy. *Nano Lett.* **2018**, 18, 3313–3321.
4. Lim, C.H.Y.X., Sorkin, A., Bao, Q., Li, A., Zhang, K., Nesladek, M. and Loh, K.P. A hydrothermal Anvil made of Graphene Nanobubbles on Diamond. *Nat. Commun.* **2013**, 4, 1556.
5. Wang, C., Qiao, Q., Shokuhfar, T. & Klie, R. F. High-Resolution Electron Microscopy and Spectroscopy of Ferritin in Biocompatible Graphene Liquid Cells and Graphene Sandwiches. *Adv. Mater.* **2014**, 26, 3410–3414.
6. Hu, X., Yasaei, P., Jokisaari, J., Öğüt, S., Salehi-Khojin, A. and Klie, R.F. Mapping Thermal Expansion Coefficients in Freestanding 2D Materials at the Nanometer Scale. *Phys. Rev. Lett.* **2018**, 120, 55902.
7. White, E. R., Mecklenburg, M., Shevitski, B., Singer, S. B. & Regan, B. C. Charged Nanoparticle Dynamics in Water Induced by Scanning Transmission Electron Microscopy. *Langmuir.* **2012**, 28, 3695–3698.
8. He, K., Nie, A., Yuan, Y., Ghodsi, S.M., Song, B., Firlar, E., Lu, J., Lu, Y.P., Shokuhfar, T., Megaridis, C.M. and Shahbazian-Yassar, R. In Situ Transmission Electron Microscopy Explores a New Nanoscale Pathway for Direct Gypsum Formation in Aqueous Solution. *ACS Appl. Nano Mater.* **2018**, 1, 5430–5440.
9. Ribeiro, A.R., Mukherjee, A., Hu, X., Shafien, S., Ghodsi, R., He, K., Gemini-Piperni, S., Wang, C., Klie, R.F., Shokuhfar, T. and Shahbazian-Yassar, R. Bio-Camouflage of Anatase Nanoparticles Explored by In Situ High-Resolution Electron Microscopy. *Nanoscale.* **2017**, 9, 10684–10693.
10. Bergmann, U., Wernet, P., Glatzel, P., Cavalleri, M., Pettersson, L.G.M., Nilsson, A. and Cramer, S.P. X-ray Raman Spectroscopy at the Oxygen K Edge of Water and Ice: Implications on Local Structure Models. *Phys. Rev. B.* **2002**, 66, 92107.
11. Garvie, L. A. J. & Buseck, P. R. Ratios of Ferrous to Ferric Iron from nanometre-Sized Areas in Minerals. *Nature.* **1998**, 396, 667.
12. Egerton, R. F. Electron Energy-Loss Spectroscopy in the electron microscope; Springer Science & Business Media: New York, 2011; pp 231-288.

13. Lupi, L., Kastelowitz, N. & Molinero, V. Vapor Deposition of Water on Graphitic Surfaces: Formation of Amorphous Ice, Bilayer Ice, Ice I, and Liquid Water. *J. Chem. Phys.* **2014**, 141, 18C508.

14. Kastelowitz, N. & Molinero, V. Ice–Liquid Oscillations in Nanoconfined Water. *ACS Nano.* **2018**, 12, 8234–8239.

15. Pauling, L. The Structure and Entropy of Ice and of other Crystals with some Randomness of Atomic Arrangement. *J. Am. Chem. Soc.* **1935**, 57, 2680–2684.

16. Onsager, L. & Dupuis, M. The Electrical Properties of Ice. *Rend. deUa ScuoIa Internazionale di Fis. "E. Fermi", Corso.* **1960**, 10, 294.

17. Koga, K., Tanaka, H. & Zeng, X. C. First-Order Transition in Confined Water Between High-Density Liquid and Low-Density Amorphous Phases. *Nature.* **2000**, 408, 564.

18. Koga, K., Zeng, X. C. & Tanaka, H. Freezing of Confined Water: A Bilayer Ice Phase in Hydrophobic Nanopores. *Phys. Rev. Lett.* **1997**, 79, 5262.